On Hydraulic Performance of Bottom Diversion Works

Hiroji NAKAGAWA

Introductory Statement

The rapid growth of industries, increase of urban population and intense land-utilization around cities have recently demanded not only the development of plans for water-resources but also the improvement of the hydraulic structures which command the service of the river water.

Although various kinds of structures to branch the flow are in use, such as fixed or movable weirs, bottom racks, dividing channels etc, each of which shows a peculiar hydraulic performance, the studies in this field have hitherto laid emphasis on the practical analysis of flow profile along the diversion works and model investigations on the individual problem from the point of view of hydraulic design. Therefore, most of the analytical methods have been developed on the basis of empirical assumptions and the results obtained by the existing method of analysis only show a rough coincidence with the actual phenomena.

From the standpoint mentioned above, the hydraulic behaviour of a spatially varied flow with a decreasing discharge is investigated herein.

1. General Remarks

The behaviour of open-channel flow on the diversion works is usually analysed by the theory of the gradually varied flow with non-uniform discharge. As to the flow with increasing discharge, many investigators have developed[1],[2],[3],[4],[5],[6] a method for the practical analysis of the flow profiles with respect to the hydraulic design of the side channel spillway, wash-water trough and side ditch of the road. These analyses are based on the one-dimensional momentum principle without exception, because the energy loss due to the turbulent mixing of the added water is uncertain. Homma[7] treated the flow in the road ditch on the assumption that the kinetic energy of the added water was equal to the energy loss due to the turbulent mixing. All of the expressions for the spatially varied flow developed hitherto are rather incomplete regarding the process of its derivation or its solution.

On the other hand, a flow with decreasing discharge may be treated by the energy equation according to the notion that the diverted water does not affect the energy head of the main flow. De Marchi[8] published a theory developed from the assumption of constant specific energy along the lateral weir and proved that three possible flow profiles appeared, which are different with a shooting, tranquil and critical flow. This theory was further verified experimentally by Gentiline[9]. Noseda[10] performed thoretical and experimental studies on the flow passing on a bottom rack on the same assumption as De Marchi's. This type of flow was treated theoretically by Kuntzmann and Bouvard[11] and by Frank[12] on the assumption that the total energy head was constant along

the rack. As investigated above, the energy change of the flow along the diverted works remains uncertain.

Accordingly, the author clarifies, mainly by experiment on the bottom diversion works, the characteristics of various elements included in the fundamental equations of a spatially varied flow with a decreasing discharge, researches the general properties of the flow profiles given by one-dimensional analysis, with the method of singular point, and discusses the applicability of the theory of the gradually varied flow.

2. Fundamental Equations

(1) Momentum analysis

When the momentum principle is applied to the spatially varied flow of steady motion, the following relationship is obtained in terms of the Cartesian coordinate system[13].

$$\frac{d}{dx}\int u^2 dA + \int u_b u_{nb} ds = \int g\sin\theta dA - \int \frac{1}{\rho}\frac{\partial}{\partial x}(p+\rho\overline{u'u'})dA - \int \frac{\tau_{xb}}{\rho}ds. \qquad (2\text{-}1)$$

where u is the velocity component in x-direction; u_b is the velocity component normal to the boundary; s is the wetted perimeter; τ_{xb} is the boundary shearing stress in x-direction. Now, representing the pressure term as a sum of hydrostatic pressure term and variation from it, $p+\rho\overline{u'u'}=\rho g(h-y)+\Delta p$.

From the continuity equation the rate of outflow per elementary length dx of the diversion structure, q_* is given by $q_* = -dQ/dx = \int u_{nb} ds$. Thus, $\int u_b u_{nb} ds = q_* u_b$. The shearing term $\int (\tau_{xb}/\rho)ds$ is given approximately by $\tau A/\rho R$.

Substituting the above equations in Eq. (2-1) and simplifying by use of the momentum coefficient β give the equation of the flow profile as

$$\frac{dh}{dx} = \frac{\sin\theta - \dfrac{\tau}{\rho g R} + \dfrac{\beta Q^2}{gA^3}\dfrac{\partial A}{\partial x} - \dfrac{Q^2}{gA^2}\dfrac{\partial\beta}{\partial x} + \dfrac{\beta Q q_*}{gA^2}\left(2-\dfrac{u_b}{\beta u_m}\right) - \dfrac{1}{gA}\int\dfrac{d}{dx}\left(\dfrac{\Delta p}{\rho}\right)dA}{\cos\theta - \dfrac{\beta Q^2}{gA^3}\dfrac{\partial A}{\partial h} + \dfrac{Q^2}{gA^2}\dfrac{\partial\beta}{\partial h}} . \qquad (2\text{-}2)$$

This becomes the equation for a gradually varied flow of constant discharge when the fifth term of the numerator, in which $(2\beta Q q_*/gA^2)$ and $-(Q q_* u_b/gA^2 u_m)$ represent the magnitude of the momentum change of the main flow and of effluent momentum respectively, is omitted.

The experiments on three kind of bottom diversion orifices shown in Fig. 2-1 were conducted to clarify the effect of each term in Eq. (2-2) on the analysis of the flow profile. The values of $p=2-(u_b/\beta u_m)$ calculated from Eq. (2-2) using the observed water surface gradients are plotted against the diversion ratio of the discharge, κ, in Fig. 2-2. Since the accuracy of the calculation of p depends on that of the measurement of the flow profile which is relatively low due to water surface oscillation, the plotted values of p scatter in so wide range as not to find the obvious correlation with κ. Neverthless, they tend to decrease proportionally to the variation of the discharge in the case of the shooting flow for the C-type diversion which has a relatively small opening per unit length, while they take a nearly constant value in the whole reach in the case of the tranquil flow. The mean value of p for this type of diversion
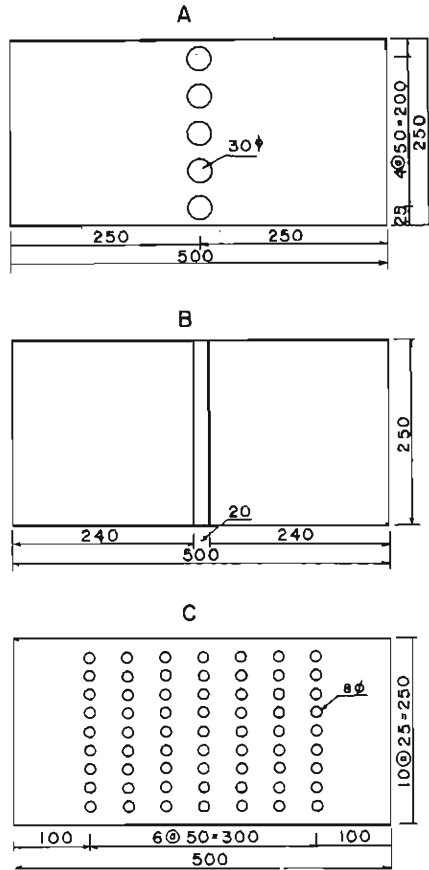
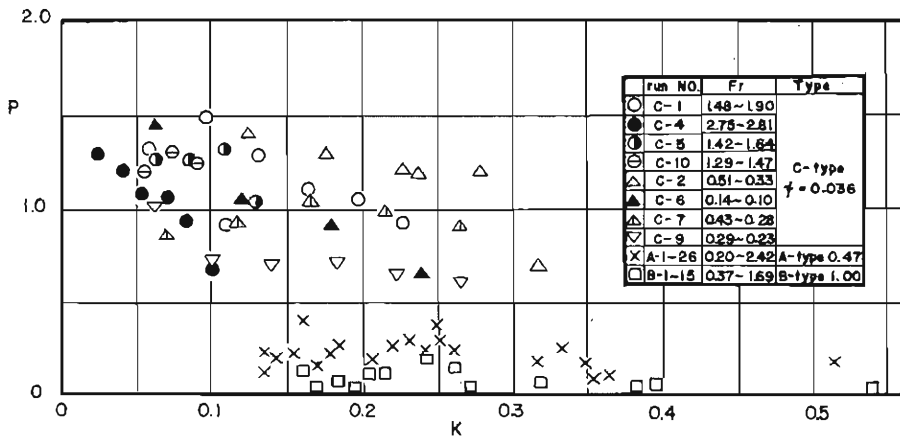Fig. 2-1. Types of bottom diversion rack and orifices used for tests.

Fig. 2-2. Variation of coefficient of momentum change against decreased discharge.
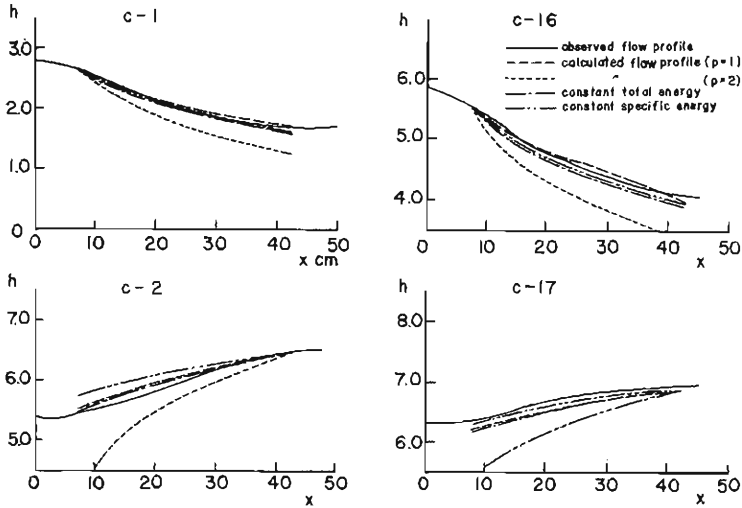
Fig. 2-3. Comparison of theoretical flow profiles and observed ones.

becomes unit, and then the effluent momentum can not be disregarded even for the gradually varied flow. This fact is verified by the observation of the flow profiles as shown in Fig. 2-3.

(2) Energy analysis

As done in the momentum analysis, the following equation of the steady flow about the Cartesian co-ordinate can be obtained on the principle of energy conservation,

$$\frac{d}{dx}\int\left\{\frac{u^2}{2}+\frac{1}{\rho}(p+\overline{u'u'})+g\,y\cos\theta+\Omega_b\right\}u\,dA=$$
$$-\int\left\{\frac{u_b^2}{2}+\frac{1}{\rho}(p_b+\overline{u'u_b'})+\Omega_b\right\}u_{nb}\,ds-\int\frac{\tau_{xb}u_b}{\rho}\,ds. \qquad (2\text{-}3)$$

where Ω_b is the potential of the channel bed; y is the shortest distance from the bed; subscript b represents the values on the boundary surface. Substituting the energy coefficient $\alpha(=(1/A)\int(u^3/u_m^3\,dA))$, the pressure coefficient $\lambda(=(1/Qh\cos\theta)\int\{\cos\theta\cdot h+(\Delta p/\rho g)\}u\,dA)$ and the equation $\partial\Omega_b/\partial x=-g\sin\theta$ in Eq. (2-3) and simplifying,

$$\frac{dh}{dx}=\frac{\sin\theta-\dfrac{\tau}{\rho gR}\dfrac{u_b}{u_m}-\dfrac{Q^2}{2gA^2}\dfrac{\partial\alpha}{\partial x}-h\cos\theta\dfrac{\partial\lambda}{\partial x}+\dfrac{Q^2}{2gA^2}\dfrac{\partial\alpha}{\partial h}+\dfrac{\alpha Qq_*}{gA^2}\left(\dfrac{3}{2}-\dfrac{u_b^2}{2\alpha u_m^2}\right)-\dfrac{q_*}{Q}\dfrac{\Delta p_b}{\rho g}}{\lambda\cos\theta-\dfrac{Q^2}{gA^3}\dfrac{\partial A}{\partial h}+h\cos\theta\dfrac{\partial\lambda}{\partial h}+\dfrac{Q^2}{2gA^2}\dfrac{\partial\alpha}{\partial h}}.$$

$$(2\text{-}4)$$

As the energy change of the main flow per unit length due to a decrease of discharge is $\rho g q_*\{(3\alpha u_m^2/2g)+\lambda h\cos\theta+(\Omega_b/g)\}$ and the effluent energy is $-\rho g q_*\{(u_b^2/2g)+h_b\cos\theta+(\Omega_b/g)+(\Delta p_b/\rho g)\}$. Eq. (2-4) is equal to that of constant discharge to which $(q_*/Q)\{(2\alpha u_m^2-u_b^2)/2g+(\lambda-1)h\cos\theta+(\Delta p_b/\rho g)\}$ is added in the numerator.

On analysis of the flow with decreasing discharge, the work done by the pressure at the outlet is expected to occur for the energy loss due to the turbulent mixing which is conceived in the flow of constant discharge. Then, though a decrease of the mean flow energy due to an increase of the turbulence and to occurrence of the eddies may of course arise in such a kind of flow, it is nearly impossible to estimate their magnitude both theoretically and experimentally. From a comparison of the computed flow profile with the observed one, it is concluded that the kinetic energy of the mean flow is fairly maintained at the outlet as it is.

Eq. (2-2) is entirely different from Eq. (2-4) in its representation, though both represent the sole phenomenon. It is difficult to decide which equation has to be used for analysis, because various assumptions given for one-dimesional analysis are very approximate to the actual phenomena. Neverthless, it is generally agreed that the momentum analysis which includes fewer uncertainties may be more useful than the energy analysis even for the bend flow with a rapidly decreasing discharge, while the energy analysis might not be applicable to the local flow with the remarkable three-dimensional characteristics because the assumptions that the flow is one-directional and that variant velocity from the mean is small to be negligible are induced. In any case, in order to raise the accuracy of analysis of the flow profile it is necessary to disclose the variation of the coefficients included in the flow profile equation with the decrease of the discharge.

3. Variation of the Coefficients Included in the Flow Profile Equations
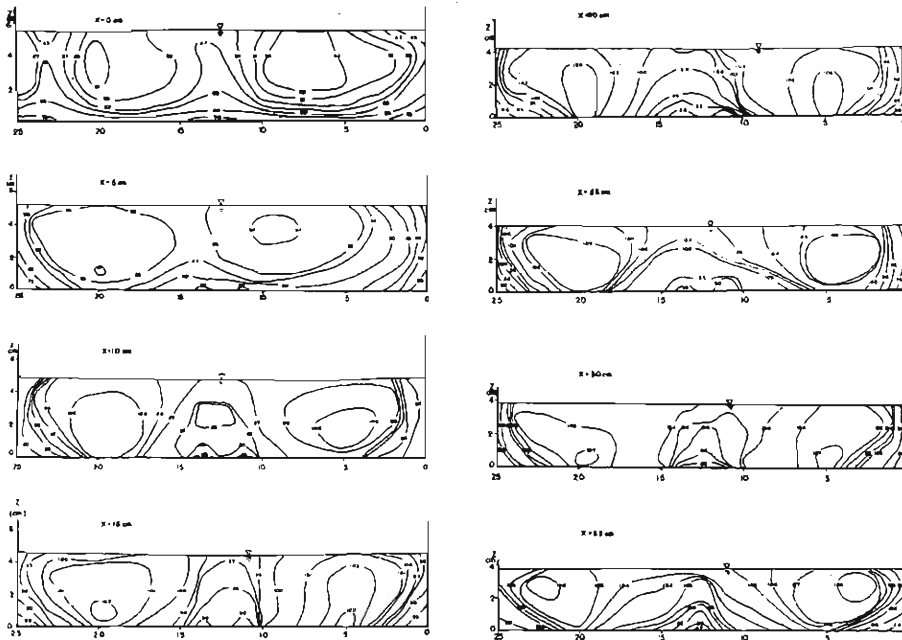

Fig. 3-1. Isovels of shooting flow.

To analyse the flow profile by use of Eq. (2-2) or (2-4), the shearing stress, the velocity correct factors, the pressure coefficients and the withdrawn discharge must be clarified. The theoretical treatment of the shearing stress might be impossible unless the variation of the internal mechanism of flow with a decrease of the discharge is solved, while the resistance law could not be established because the actual change of the flow profile might be influenced by the variation of the other uncertain elements. Here the resistance factors which have been empirically determined for the flow of constant discharge are used in the equations.

(1) The velocity-distribution coefficients

Isovels of the shooting and tranquil flow passing on the bottom diversion orifices, type C, are shown in Fig. 3-1 and 3-2, respectively. Regardless of
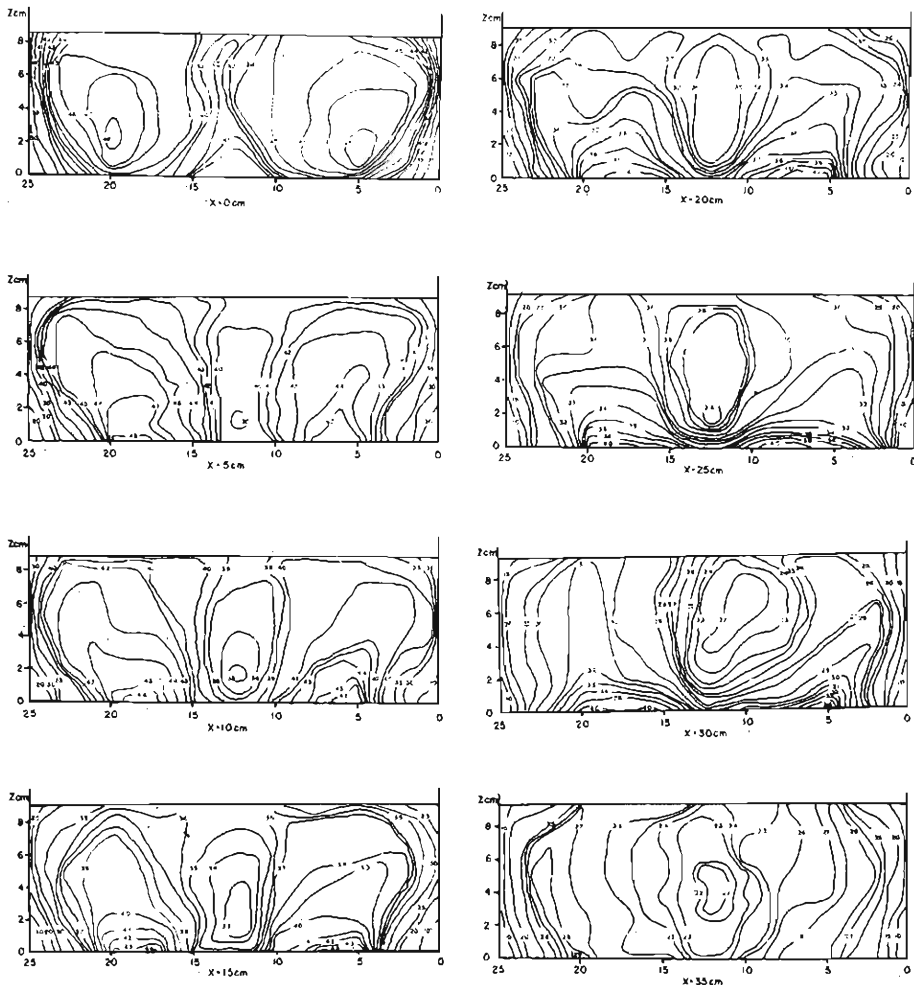

Fig. 3-2. Isovels of tranquil flow.

flow condition two points which show the maximum velocity appear near each side of the channel at any one section.   When the water depth is relatively large, these predominant flow regions begin to develop close to both sides from the entrance of the outflow section.   However, in the case of small depth the predominant regions which lie in the neighbourhood of the water surface at the upstream end of the diversion structure gradually shift downstream toward both the channel bottom and side walls.   The occurrence of two predominant flow regions in one cross-section which was also observed in other author's experiments might be due to the secondary flow caused by the uneven distri-

TABLE 3-1.
Coefficients of velocity distribution and the specific energy.

Types of diversion	Run No.	x (cm)	κ	α	β	H (cm)	H/H_0
Side Weir	5-0-20-6-T	12.5	0.025	1.051	1.020		
		50.0	0.144	1.090	1.038	8.25	
		100.0	0.356	1.188	1.107	8.07	
		187.5	0.819	1.772	1.575	7.90	
	10-0-30-5-T	12.5	0.016	1.081	1.029		
		50.0	0.067	1.086	1.034	12.43	
		100.0	0.149	1.112	1.040	12.49	
		187.5	0.365	1.171	1.068	12.79	
	5-1-21-0-S	0	0	1.047	1.007	15.81	1.000
		10.0	0.056	1.020	1.006	15.42	0.975
		20.0	0.100	1.025	1.012	15.02	0.950
		30.0	0.143	1.042	1.018	15.12	0.956
		40.0	0.190	1.020	1.012	14.69	0.929
Bottom Back	C-16-S	-2.5	0	1.027	1.015	9.27	1.000
		2.5	0.064	1.020	1.013	9.10	0.983
		17.5	0.103	1.018	1.013	9.09	0.981
		27.5	0.140	1.013	1.009	9.05	0.977
	C-1-S	-2.5	0	1.031	1.017	5.25	1.000
		2.5	0.041	1.050	1.028	5.21	0.992
		17.5	0.239	1.018	1.012	5.10	0.972
	C-2-T	-2.5	0	1.046	1.023	6.72	1.000
		7.5	0.107	1.086	1.039	6.70	0.997
		17.5	0.224	1.121	1.044	6.83	1.017
		27.5	0.352	1.132	1.048	6.89	1.024
	C-17-T	-2.5	0	1.095	1.039	7.30	1.000
		12.5	0.133	1.122	1.042	7.37	1.010
		17.5	0.220	1.149	1.050	7.34	1.005
		27.5	0.334	1.158	1.053	7.28	0.998
		32.5	0.391	1.196	1.072	7.25	0.994

bution of the withdrawn discharge which differs between the central part and the corner of the cross-section.

The energy coefficient α is represented in consideration not only of the velocity component parallel to the channel u, but the normal components v and w, as follows;

$$\alpha = \frac{1}{A} \int_A \left(\frac{u}{u_m}\right)^3 \left\{1 + \left(\frac{v}{u}\right)^2 + \left(\frac{w}{u}\right)^2\right\} dA. \tag{3-1}$$

The momentum coefficient β is given as

$$\beta = \frac{1}{A} \int_A \left(\frac{u}{u_m}\right)^2 dA. \tag{3-2}$$

In the analysis of the flow profile on the bottom rack the v-component may be neglected as two-dimensional flow.
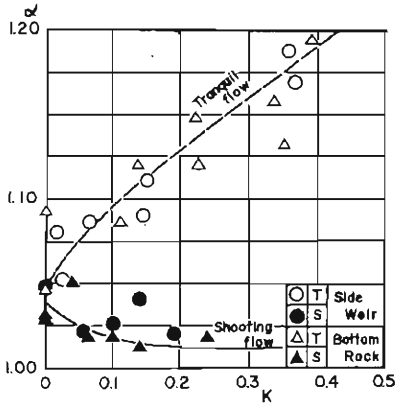

Fig. 3-3. Variation of velocity-distribution coefficient along the channel.

The values α and β computed by means of Eqs. (3-1) and (3-2) from the author's experimental data on side weirs and bottom diversion racks are shown in Table 3-1. Values of α are plotted against the corresponding values of the diverted discharge ratio κ in Fig. 3-3. From this figure it is noted that in a supercritical flow the values of α decrease along the channel so that use of the mean velocity will give fair accuracy, while in a subcritical flow they rapidly increase with the values of κ, since the variation of the discharge might sensitively influence the velocity distribution.

The fact that each diversion structure takes a nearly equal value of α for the same flow condition and diverted discharge ratio is very interesting.

(2) *The pressure coefficient*

A two-dimensional open channel flow passing over the bottom diversion work will be treated herein. Let x be the distance along the channel bottom measured in the direction of mean flow; z is the distance from the bottom; u and w are the velocity components in each direction; p is the average pressure. Assuming that $\partial^2 u/\partial x^2 \ll \partial^2 u/\partial z^2$, $\partial^2 w/\partial x$ and $\partial^2 w/\partial z^2 \ll \partial^2 u/\partial z^2$, the equations of motion in each direction can be written as

$$u\frac{\partial u}{\partial x} + w\frac{\partial u}{\partial z} = g\sin\theta - \frac{1}{\rho}\frac{\partial p}{\partial x} + \nu\frac{\partial^2 u}{\partial z^2}, \tag{3-3}$$

$$u\frac{\partial w}{\partial x} + w\frac{\partial w}{\partial z} = -g\cos\theta - \frac{1}{\rho}\frac{\partial p}{\partial z}. \tag{3-4}$$

The equation of continuity is

$$\frac{\partial u}{\partial x} + \frac{\partial w}{\partial z} = 0. \tag{3-5}$$

Substituting Eq. (3-5) in Eq. (3-3) and (3-4), and simplifying, they will be written in the following forms.

$$-\frac{u^2}{g}\frac{\partial(w/u)}{\partial z}=\sin\theta-\frac{1}{\rho g}\frac{\partial p}{\partial x}+\frac{\nu}{g}\frac{\partial^2 u}{\partial z^2}\,,\tag{3-6}$$

$$\frac{u^2}{g}\frac{\partial(w/u)}{\partial z}=-\cos\theta-\frac{1}{\rho g}\frac{\partial p}{\partial z}\,.\tag{3-7}$$

If the distribution pattern of u-components might be conservative in the direction of the main flow, the following expression will be obtained,

$$u=u_m f'(z/h)=(q/h)f'(m).\tag{3-8}$$

where u_m is the mean velocity and q is the discharge of the main flow per unit width of the channel.

Substituting Eq. (3-8) in Eq. (3-5) and integrating, w component in z direction can be obtained by use of the free surface condition, $w/u=dh/dx$, and of the continuity equation, $dq/dx=-q_{**}$, as follows

$$w=q_{**}\{f(m)-f(1)\}+(qm/h)(dh/dx)f'(m).\tag{3-9}$$

Substituting Eqs. (3-8) and (3-9) in Eq. (3-7) and integrating from z to h, the equation of the pressure distribution is obtained as follows

$$\begin{aligned}
\frac{p}{\rho g}&=(1-m)h\cos\theta+\frac{q^2{}_{**}}{g}\int_m^1 f'(m)\{f(m)-f(1)\}dm+\frac{1}{g}\frac{dh}{dx}\\
&\times\Big[q\frac{dq_{**}}{dh}\int_m^1 f'(m)\{f(m)-f(1)\}dm-\frac{qq_{**}}{h}\int_m^1 m\{f'(m)\}^2dm\\
&+\frac{qq_{**}}{h}\int_m^1 f'(m)\{f(m)-f(1)\}dm+\frac{qq_{**}}{h}\int_m^1 mf'(m)\{f(m)-f(1)\}dm\Big]\\
&-\frac{q^2}{gh^2}\Big(\frac{dh}{dx}\Big)^2\int_m^1 m\{f'(m)\}^2dm+\frac{q^2}{gh}\frac{d^2h}{dx^2}\int_m^1 m\{f'(m)\}dm.
\end{aligned}\tag{3-10}$$

When the velocity component in x-direction at any section can be expressed as the mean velocity u_m, the following equations are satisfied;

$$du/dz=0,\quad f'(m)=1,\quad f(m)=m,\quad f(1)=1,\quad f''(m)=0.\tag{3-11}$$

Representing the rate of outflow per unit width of the channel, q_{**}, as $C_h\psi\sqrt{2gh}$ and assuming the discharge coefficient to be constant, dq_{**}/dh becomes equal to $q_{**}/2h$. Using the above expressions, Eq. (3-10) becomes

$$\begin{aligned}
\frac{p}{\rho g}&=(1-m)h\cos\theta-(1-m^2)\frac{q^2{}_{**}}{2g}-(5-m)(1-m)\frac{qq_{**}}{4gh}\frac{dh}{dx}\\
&-(1-m^2)\frac{q^2}{2gh^2}\Big(\frac{dh}{dx}\Big)^2+(1-m^2)\frac{q^2}{2gh}\frac{d^2h}{dx^2}\,.
\end{aligned}\tag{3-12}$$

The left side of this equation consists of the hydrostatic term, the term of the pressure degenerated by the outflow and the pressure change brought by the gradient and curvature of the water surface.

The pressure head at the bottom, $p_b/\rho g$, is obtained by taking $m=0$ for Eq. (3-12),

$$\frac{p_b}{\rho g} = h\cos\theta - \frac{q^2_{**}}{2g} - \frac{5qq_{**}}{4g\overline{h}}\frac{dh}{dx} - \frac{q^2}{2gh^2}\left(\frac{dh}{dx}\right)^2 + \frac{q^2}{2g\overline{h}}\left(\frac{d^2h}{dx^2}\right). \tag{3-13}$$

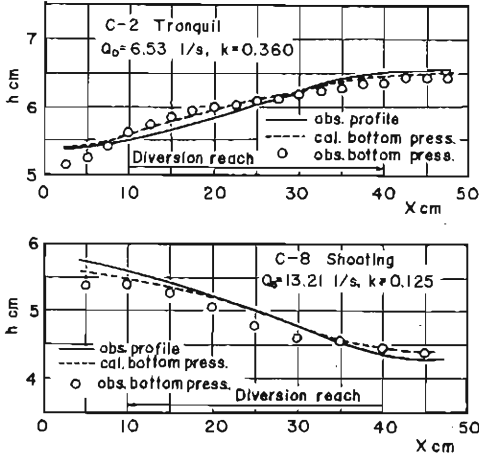The bottom pressure distributions along the bottom diversion orifice of type C, computed by use of the observed values of dh/dx and d^2h/dx^2, are shown in Fig. 3-4, and compared with the measured values. The sign of the non-hydrostatic pressure term in Eq. (3-13) usually depends on that of (d^2h/dx^2), because the values of the last term on the right side give a higher order than the others. For a tranquil flow condition the convex upwards profile near the entrance of the diversion yields the subhydrostatic bottom pressure as shown in Fig. 3-4, while near the end of the diversion the super-hydrostatic bottom pressure is given due to the negative value of d^2h/dx^2. For a shooting flow condition this relationship is reversed.

Fig. 3-4. Flow profiles and bottom pressures on diversion work.

The pressure coefficients based on energy and momentum analysis are expressed, respectively, by

$$\lambda = 1 + \frac{1}{Qh\cos\theta}\int\frac{\Delta p}{\rho g}\,u\,dA, \tag{3-14}$$

$$\lambda' = 1 + \frac{1}{Az_G\cos\theta}\int\frac{\Delta p}{\rho g}\,dA, \tag{3-15}$$

where Δp is the variation from the hydrostatic pressure, and z_G is the distance from the water surface to the center of gravity of the flow cross-section.

Substituting Eq. (3-11) in Eqs. (3-14) and (3-15) and integrating from 0 to 1 for m, the pressure coefficients for two-dimensional flow on the bottom diversion rack are reduced, repetively, to,

$$\lambda = 1 - \frac{1}{6gh\cos\theta}\left\{q^2_{**} + \frac{7qq_{**}}{2h}\frac{dh}{dx} - \frac{2q^2}{h^2}\left(\frac{dh}{dx}\right)^2 - \frac{2q^2}{h}\frac{d^2h}{dx^2}\right\}, \tag{3-16}$$

$$\lambda' = 2\lambda - 1. \tag{3-17}$$

The variations of the pressure coefficients along the diversion works will be discussed in the later chapter in relation of the flow characteristics at the quasi-saddle point.

(3) The specific energy

For practical analysis of a spatially varied flow with decreasing discharge the assumption that the specific energy is constant along the channel has been used as shown by De Marchi. The specific energy is defined as

$$H_0 = \frac{1}{Q} \int \left\{ \frac{1}{2g}(u^2 + v^2 + w^2) + \frac{p}{\rho g} + z \cos \theta \right\} u dA = \frac{\alpha u^2_m}{2g} + \lambda h \cos \theta. \qquad (3\text{-}18)$$

The values of specific energy and its distribution along the channel obtained by experiments are shown in Table 3-1. For a supercritical flow the specific energy decreases along the channel, while for a subcritical flow it slightly increases or at least is constant. The ratios of the specific energy at the end of the weir section, H_2, to that at the entrance, H_0, for a supercritical flow which were obtained by experiments with side weirs of 3 cm and 5 cm heights, are plotted in Fig. 3-5 against the mean Froude number of the flow at the entrance. It is found that the reduction rate of the specific energy becomes larger in proportion to the initial Frounde number of the flow. From the viewpoint mentioned above it is concluded that the assumption of constant specific energy is inadequate for an analysis of the supercritical flow.
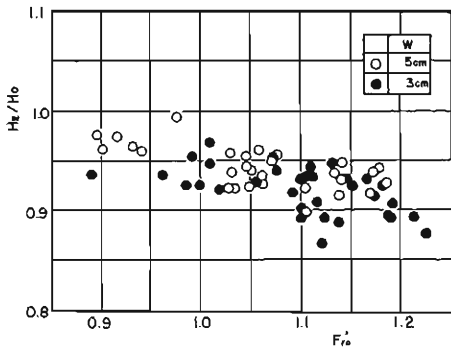

Fig. 3-5. Reducing characteristics of the specific energy along the side weir with initial Froude number.
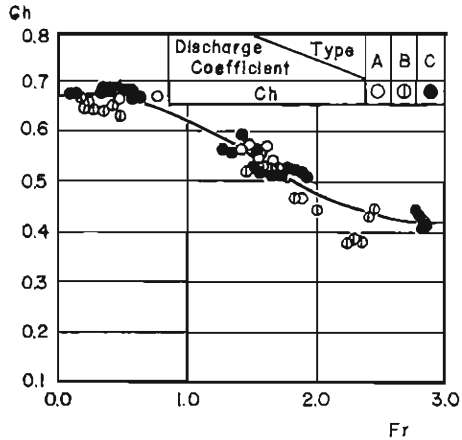
Fig. 3-6. Coefficient of withdrawn discharge for bottom rack.

(4) The withdrawn discharge

The discharge through unit length of the bottom rack and orifice shown in Fig. 2-1 may be expressed by

$$q_{**} = C_h B \psi \sqrt{2gh}, \qquad (3\text{-}19)$$

where C_h is the coefficient of discharge through the openings and ψ is the ratio of the opening area to the total area of the rack surface.

The values C_h of the coefficient of discharge through the opening determined experimentally are plotted in Fig. 3-6 against the Froude number of the main flow averaged at the discharging section. It is concluded that the value C_h is nearly constant for a subcritical flow, whereas it decreases for a supercritical flow as the value F_r increases, and that the racks of transverse bars and of circular orifices show the same value of C_h for any Froude number.

4. Flow Profiles Near Singular Points

(1) The features of the fundamental equations

The theoretical analysis of the spatially varied flow with decreasing discharge is carried out by use of the theory of the singular point[14].

The fundamental equations of the gradually varied steady flow with decreasing discharge are given from Eq. (2-2) by use of the parameter ζ as

$$\frac{dh}{d\zeta} = \sin\theta - \frac{\tau}{\rho gR} - \frac{\alpha Q^2}{gA^3}\frac{\partial A}{\partial x} + \frac{\alpha p q_* Q}{gA^2} , \qquad (4\text{-}1)$$

$$\frac{dx}{d\zeta} = \cos\theta - \frac{\alpha Q^2}{gA^3}\frac{\partial A}{\partial h} , \qquad (4\text{-}2)$$

$$\frac{dQ}{d\zeta} = -q_*\left(\cos\theta - \frac{\alpha Q^2}{gA^3}\frac{\partial A}{\partial h}\right). \qquad (4\text{-}3)$$

The method of analysis varies according to whether the withdrawn discharge q_* is dependent on the flow depth h or the travelling distance x, or both of them, as shown in Table 4-1. Since a diversion structure with uniform channel and constant opening area is used in most cases, q_* only depends on the flow depth, and the flow profile can be treated as a two-dimensional problem in the $Q-h$ phase plane.

TABLE 4-1.

Classification of the spatially varied flows with decreasing discharge.

Function of withdrawn discharge	Uniformity of channel	Method of analysis	Example
$q_*=$const.	uniform	$Q-h$, $x-h$ pl.	Diversion with uniform decrease of discharge
$q_*=$const.	not uniform	$x-h$ pl.	〃
$q_*=q_*(h)$	uniform	$Q-h$ pl.	Diversion with constant ratio of opening
$q_*=q_*(h)$	not uniform	$Q-h-x$ pl.	〃
$q_*=q_*(x)$	uniform	$x-h$ pl.	Diversion with arbitrary decreasing rate of discharge
$q_*=q_*(x)$	not uniform	$x-h$ pl.	〃
$q_*=q_*(x, h)$	uniform	$Q-h-x$ pl.	Diversion with variable ratio of opening
$q_*=q_*(x, h)$	not uniform	$Q-h-x$ pl.	〃

(2) The flow behaviour near singular points (two-dimensional problem)

When the channel is uniform and $q_*=q_*\,(Q, h)$, the fundamental equations of flow profile for a rectangular channel which do not contain x directly are given as

$$\frac{dh}{d\zeta} = \sin\theta - \frac{n^2 Q^2}{R^{4/3}B^2 h^2} + \frac{\alpha p q_* Q}{gB^2 h^2} \equiv f_1(Q, h), \qquad (4\text{-}4)$$

$$\frac{dQ}{d\zeta} = -q_*\left(\cos\theta - \frac{\alpha Q^2}{gB^2 h^3}\right) \equiv f_2(Q, h). \qquad (4\text{-}5)$$

Since $f_1 \equiv f_2 \equiv 0$ at the singular point, the relationships are given as

$$\sin \theta = \frac{n^2 Q_c^2}{R_c^{4/3} B^2 h_c^2} - \frac{\alpha p_c q_{*c} Q_c}{g B^2 h_c^2} ,$$ (4-6)

$$\cos \theta = \frac{\alpha Q_c^2}{g B^2 h_c^3} ,$$ (4-7)

where subscript c represents the values at the singular point. When Eq. (4-6) is divided by Eq. (4-7), the following equation is obtained by use of the relation $i = \tan \theta$;

$$\frac{i_b}{h_c} = \frac{g n^2}{\alpha R_c^{4/3}} - \frac{q_{*c} p_c}{Q_c} .$$ (4-8)

To examine the flow characteristics at the singular point, transferring the origin of Eq. (4-4) and (4-5) to the singular point and neglecting the minute quantities above the second order, the fundamental equations approximate to the linear differential equations on the assumption that α and p are constant;

$$\left. \begin{array}{l} \dfrac{dQ'}{d\zeta'} = a_{11}Q' + a_{12}h' \\[2mm] \dfrac{dh'}{d\zeta'} = a_{21}Q' + a_{22}h' \end{array} \right\} ,$$ (4-9)

where the numerical constants a_{11}, a_{12}, a_{21}, and a_{22} are given as

$$\left. \begin{array}{l} a_{11} = \dfrac{2q_{*c} \cos \theta}{Q_c}, \qquad a_{12} = -\dfrac{3q_{*c} \cos \theta}{h_c} \\[3mm] a_{21} = -\dfrac{2h_c \cos \theta}{Q_c^2} \left\{ \dfrac{i_b Q_c}{h_c} + \dfrac{p_c q_{*c}}{2} - \dfrac{p_c Q_c}{2} \left(\dfrac{\partial q_*}{\partial Q} \right)_c \right\} \\[3mm] a_{22} = \dfrac{h_c \cos \theta}{Q_c} \left\{ \dfrac{2i_b Q_c}{h_c^2} + \dfrac{4R_c}{3h_c^2} \left(\dfrac{i_b Q_c}{h_c} + p_c q_{*c} \right) + p_c \left(\dfrac{\partial q_*}{\partial h} \right)_c \right\} \end{array} \right\} .$$ (4-10)

Since the coefficient of discharge of a bottom rack consisting of transverse bars or circular orifices depends only on the Froude number of the flow, the numerical constants are determined as

$$\left. \begin{array}{l} a_{11} = \dfrac{2q_{*c} \cos \theta}{Q_c}, \qquad a_{12} = -\dfrac{3q_{*c} \cos \theta}{h_c} \\[3mm] a_{21} = -\dfrac{2h_c \cos \theta}{Q_c^2} \left\{ \dfrac{i_b Q_c}{h_c} + \dfrac{p_c q_{*c}}{2} - \dfrac{F_{rc} p_c q_{*c}}{2C_{hc}} \left(\dfrac{\partial C_h}{\partial F} \right)_c \right\} \\[3mm] a_{22} = \dfrac{h_c \cos \theta}{Q_c} \left\{ \dfrac{2i_b Q_c}{h_c^2} + \dfrac{4R_c}{3h_c^2} \left(\dfrac{i_b Q_c}{h_c} + p_c q_{*c} \right) + \dfrac{p_c q_{*c}}{2h_c} - \dfrac{3F_{rc} p_c q_{*c}}{2h_c C_{hc}} \left(\dfrac{\partial C_h}{\partial F} \right)_c \right\} \end{array} \right\} .$$ (4-11)

As it is apparent from Fig. 3-6 that $(\partial C_h/\partial F)_c < 0$, $a_{11} > 0$, $a_{12} < 0$, $a_{21} < 0$ and $a_{22} > 0$ are satisfied.

The characteristic equation of Eq. (4-9) is given as

$$\left| \begin{array}{cc} a_{11} - \lambda & a_{12} \\ a_{12} & a_{22} - \lambda \end{array} \right| = 0.$$ (4-12)

The discriminant of Eq. (4-12) in this case shows a positive value, that is,

$$D = (a_{11} - a_{22})^2 + 4a_{12}a_{21} > 0.$$ (4-13)

And then

$$a_{11}a_{22} - a_{12}a_{21} = \frac{2q^2{}_{*c}\cos^2\theta}{Q_c{}^2}\left(\frac{4R_c}{3h_c} - 1\right)\left(\frac{i_bQ_c}{h_c} + p_cq_{*c}\right). \qquad (4\text{-}14)$$

It is concluded from Eq. (4-14) that the singular point becomes a nodal one for $h_c/B < 1/6$ and a saddle one for $h_c/B > 1/6$. And when two singular points appear in a diversion reach it is proved that the singular point on the upstream side becomes a saddle point and the one on the downstream side a nodal one, by the fact that a gradient of critical depth line is decidedly negative.

From the above research the flow profiles which appear in the neighborhood of the singular points in the diversion channel are shown in Fig. 4-1 and 4-2.
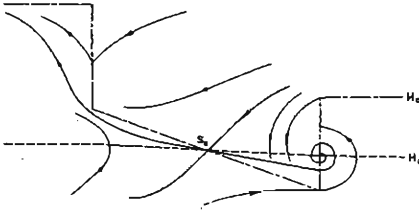

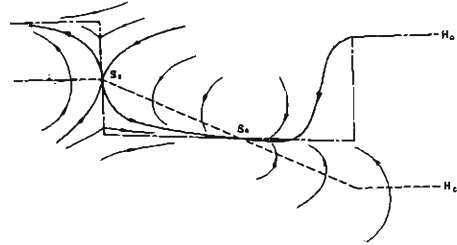Fig. 4-1. Possible flow profiles near a saddle point.

Fig. 4-2. Possible flow profiles near a quasi-saddle point and a nodal point.

(3) The flow behaviour near singular points (three-dimensional problem)

When the channel and openings are not uniform for flow direction the linear differential equations near the singular point are given as

$$\left.\begin{aligned}
\frac{dx'}{d\zeta} &= a_{11}x' + a_{12}h' + a_{13}Q' \\
\frac{dh'}{d\zeta} &= a_{21}x' + a_{22}h' + a_{23}Q' \\
\frac{dQ'}{d\zeta} &= -q_{*c}a_{11}x' - q_{*c}a_{12}h' - q_{*c}a_{13}Q'
\end{aligned}\right\}. \qquad (4\text{-}15)$$

The characteristic equation of Eq. (4-15) is expressed by

$$\begin{vmatrix} a_{11}-\lambda & a_{12} & a_{13} \\ a_{21} & a_{22}-\lambda & a_{23} \\ -q_{*c}a_{11} & -q_{*c}a_{12} & -q_{*c}a_{13}-\lambda \end{vmatrix} = 0. \qquad (4\text{-}16)$$

The solutions of Eq. (4-16) are given as

$$\begin{aligned}
\lambda_1 &= 0, \\
\left.\begin{aligned}\lambda_2, \\ \lambda_3\end{aligned}\right. &= \frac{1}{2}\left[(a_{11}+a_{22}-q_{*c}a_{13}) \pm \sqrt{(a_{11}-a_{22}-q_{*c}a_{13})^2 + 4(a_{12}a_{21}-q_{*c}a_{12}a_{23})}\right]. \quad (4\text{-}17)
\end{aligned}$$

Thus the elementary divisors are determined as

$$e_1 = 1, \qquad e_2 = 1, \qquad e_3 = \lambda(\lambda-\lambda_2)(\lambda-\lambda_3),$$

and the problem is reduced to a two-dimensional problem for the $x'-h'$ phase plane.

5. Applicability of Flow Profile Equations

(1) Hydraulic behaviour of a flow with a quasi-saddle point

When the ratio ψ in Eq. (3-19), of the opening area to the total area of the rack surface, is relatively large, as in almost all diversion structures, the critical depth line discontinuously intersects with the normal depth line at the entrance of the diversion reach and the subcritical flow in the upstream channel often changes into the supercritical flow somewhere upstream from the entrance. This critical point is called "a quasi-saddle point" which shows the same behaviour as a saddle point. The ratio h_0/h_{c0}, of the entrance depth to the critical depth and the ratios L_0/h_{c0}, in which L_0 is the distance of the critical section from the entrance, obtained by the author's tests, are shown in Table 5-1. The ratio h_0/h_{c0} decreases with increase in the value of the channel slope and the opening ratio, whereas the ratio L_0/h_{c0} increases.

TABLE 5-1.
Relative depth and location of quasi-saddle point.

Run No.	Opening ratio of rack	Bed slope	Initial discharge Q_0 (l/sec.)	Withdrawn discharge ΔQ(l/sec.)	κ (%)	h_0/h_{c0}	L_0/h_{c0}
H- 1			11.38	2.26	19.6	0.989	0.159
2			15.07	2.70	17.9	0.979	0.279
3	0.054	1/1,000	5.65	1.75	31.0	0.989	0.188
4			7.41	1.94	26.2	0.975	0.246
5			16.75	2.67	15.9	0.991	0.194
6			14.80	2.65	17.9	0.996	0
C-10			12.14	1.65	13.6	0.923	7.65
11	0.036	1/500	16.96	1.81	10.7	0.917	6.30
12			13.86	1.73	12.5	0.918	6.99
16			11.64	1.62	13.9	0.926	7.01
F- 1			18.70	4.40	23.6	0.748	3.95
2	1.000	1/1,000	11.97	3.55	29.7	0.745	3.40
3			9.88	3.34	33.8	0.730	3.65

The variation of the gradient and the curvature of the water surface along a channel with bottom circular orifices of which the opening ratio ψ is 0.054 are shown in Fig. 5-1 and 5-2, respectively. The abscissa represents the ratio x/H_{0c}, of the flowing distance from the entrance to the specifie energy at the critical section. From the figure it is noticed that the curvature of the water surface takes negative values for $\bar{x}=x/H_{0c}<0.5$ and positive for $\bar{x}\geq0.5$, and the slope of the water surface takes the minimum value at this point. Each variation for various discharges is represented by a single curve as shown in the figures as long as the channel slope and the opening ratio are specified. Using values of dh/dx and d^2h/dx^2 for any x obtained from the curves in Fig. 5-1 and 5-2 and computing λ by Eq. (3-16), variations of λ on the diversion work are shown in Fig. 5-3. The curve of $d\lambda/dx$ shows so large a value near the
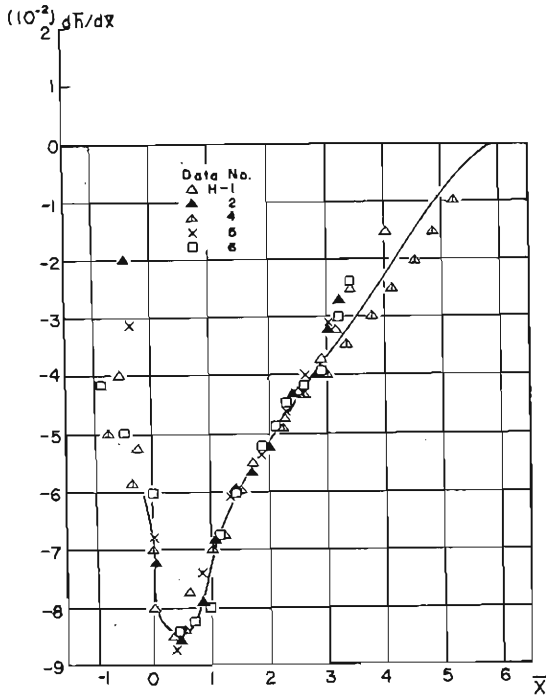
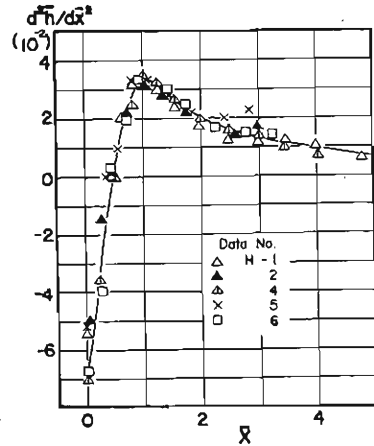Fig. 5-1.　Variation　of　water　surface　gradient　(traquil → shooting).

Fig. 5-2.　Variation　of　curvature　of water surface (tranquil → shooting).
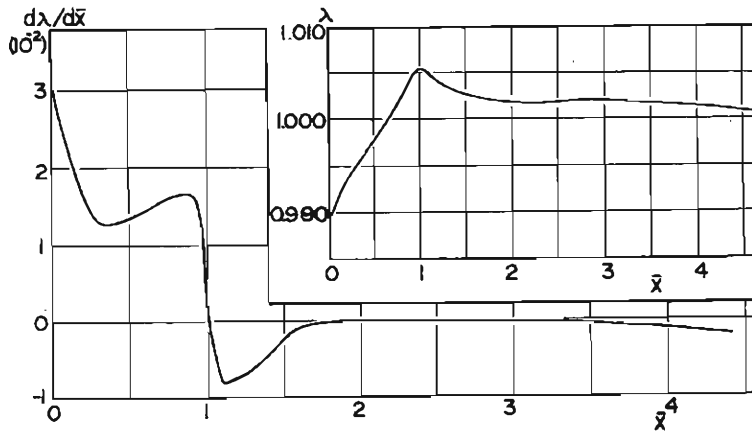

Fig. 5-3.　Variation　of　pressure　coefficient　(tranquil → shooting).

entrance that it would not be neglected in flow analysis.

It is recognized from the above description that the hydraulic behaviour of the flow at the entrance of the diversion work depends only on the initial discharge rate Q_0, that is, the critical depth in the upstream channel h_{c0}, for a

specific condition of the channel and the opening when a quasi-saddle point appears. And thus the flow characteristics at the diversion works can be found by a non-dimensional expression in respect of the specific energy at the critical section H_{0c}. The ratio C_H/C_{H0}, of the coefficient of discharge computed by the equation $q_* = C_H B \psi \sqrt{2gH_{0c}}$ at any section to that at the entrance is shown in Fig. 5-4 against $\bar{x}$. The ratio C_H/C_{H0} decreases exponentially with the increase of $\bar{x}$ represented by $C_H/C_{H0} = (1.103)^{-\bar{x}}$. Then the withdrawn discharge q_* per elementary length dx is given by
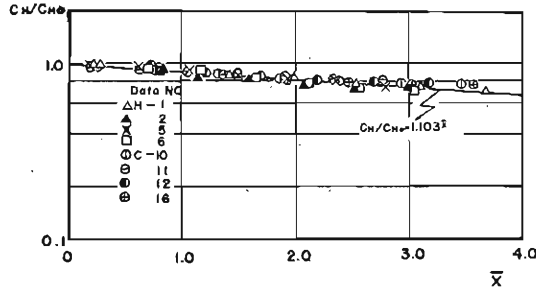

Fig. 5-4. Variation of coefficient of discharge along the channel.

$$q_* = C_{H0} B \psi \sqrt{2g\bar{H}_{0c}} (1.103)^{-\bar{x}}. \tag{5-1}$$

The ratio of the discharge withdrawn in the length of x to the initial discharge, κ, is determined using the equation $Q_0/B = (2\sqrt{2g}/3\sqrt{3})H_{0c}^{3/2}$.

$$\kappa = \frac{3\sqrt{3}}{2} \psi C_{H0} \int_0^{\bar{x}} (1.103)^{-\bar{x}} d\bar{x} = \frac{3\sqrt{3} C_{H0}\psi}{2\ln 1.103} (1 - 1.103^{-\bar{x}}). \tag{5-2}$$

There were few differences among the values of C_{H0} for various initial discharges and their mean value was 0.437. It is indicated that in this case κ is determined by only the opening ratio and the distance.

(2) *Analysis of the flow profiles*

The applicability of the flow profile equations are discussed herein, using Eq. (5-2) which expresses the discharge variation.

1) Analysis on the assumption of constant specific energy

If the specific energy of the flow is constant in the whole reach of the diversion work, the energy equation is established in the critical section, the entrance and $\bar{x}$-section on the diversion work as follows ;

$$H_{0c} = \frac{3}{2} \lambda_c h_c \cos \theta = \lambda_f h_f \cos \theta + \frac{\alpha_f Q_0^2}{2gB^2 h_f^2} = \lambda h \cos \theta + \frac{\alpha Q^2}{2gB^2 h^2} . \tag{5-3}$$

Assuming the gradually varied flow and $\alpha_f = \alpha = 1$ based on the previous investigation, the following equation can be given using the equation of continuity $Q = (1 - \kappa)Q_0$ and Eq. (5-2).

$$h \sqrt{1 - h} \cos \theta = \bar{h}_f \sqrt{1 - \bar{h}_f} \cos \theta \{1 - 11.61\psi(1 - 1.103^{-\bar{x}})\}. \tag{5-4}$$

The flow profile computed by Eq. (5-4) for $\psi = 0.0565$, and $h_f = 0.665$ is shown by the real line in Fig. 5-5. By the fact that the computed profile comes in a
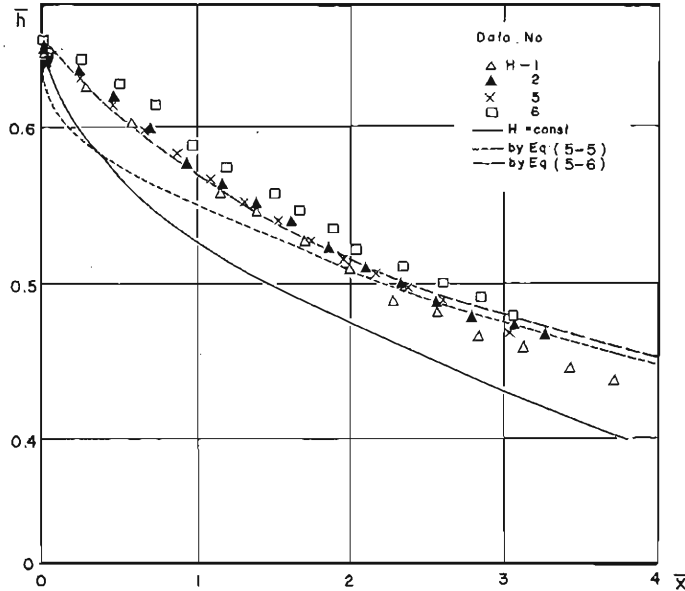
Fig. 5-4. Applicability of various wethods of flow analysis.

lower position than the observed ones in the whole reach it is proved that the specific energy decreases downstream for this kind of flow.

2) Analysis as the gradually varied flow

The flow profile equation of the gradually varied flow with a decreasing discharge for an uniform rectangular channel on the basis of a non-dimensional energy analysis is given as

$$\frac{dh}{dx} = \frac{\sin\theta - \dfrac{n^2 Q^2}{R^{4/3} B^2 \bar{h}^2} + \dfrac{\alpha p q_* Q}{g B^2 h^2}}{\cos\theta - \dfrac{\alpha Q^2}{g B^2 h^3}} . \tag{5-5}$$

Substituting Eq. (5-4) in Eq. (5-5), and using $p=1$, $\sin\theta = 1/1,000$, $n=0.01$, $\cos\theta = 1$ and $\alpha = 1$, numerical integration results in the flow profile given by the dotted line in Fig. 5-5. This is more appoximate to the observed profiles than that determined by Eq. (5-4), except near the entrance where the pressure distribution deviates from the hydrostatic one.

3) Analysis in consideration of non-hydrostatic pressure effect

The broken line shown in Fig. 5-5 represents the theoretical flow profile computed by numerical integration of the following equation ;

$$\frac{dh}{dx} = \frac{\sin\theta - \dfrac{n^2 Q^2}{R^{4/3} B^2 h^2} + \dfrac{\alpha p q_* Q}{g B^2 h^2} - h\cos\theta \dfrac{d\lambda}{dx}}{\cos\theta - \dfrac{\alpha Q^2}{g B^2 h^3}} . \tag{5-6}$$

The values of $d\lambda/dx$ in Eq. (5-6) were taken from Fig. 5-3. The theoretical curve indicates good agreement with the observed values. This fact shows

that the effect of the rapidly varied flow would be considerable in the analysis of flow profile.

6. Concluding Statement

It is very difficult to establish a general design procedure for open channel diversion works because of the great complexity of flow behaviour and the variety of structures. The present paper is intended to make clear the characteristics of the flow passing over the diversion structures on the basis of the strict hydrodynamic expression of flow behaviour with the aid of experimental and mathematical means. A complete description for the design procedure of diversion structures is not obtained by this research, but it is believed that this study gives much advanced information on the actual designing of diversion works.

As the concluding statement of this research, the following are summarized:

(1) The velocity-distribution coefficients included in the fundamental equations vary proportionally with the diverted discharge ratio κ for a subcritical flow, whereas they decrease gradually along the channel for a supercritical flow.

(2) The pressure coefficients and their gradient take such large values near the entrance of the diversion that their effect on flow analysis cannot be neglected to ensure permissible agreement with the actual phenomena.

(3) The variation of the specific energy along the channel obtained by experiments represents that it decreases along the channel for a supercritical flow, while it slightly increases or at least is constant for a subcritical flow. Therefore, it is verified that the assumption of constant specific energy as proposed by De Marchi is inadequate for the analysis of a supercritical flow.

(4) The values of the coefficient of discharge withdrawn from the bottom rack of transverse bars or circular orifices are nearly constant for a subcritical flow whereas they decrease as the Froude number increases for a supercritical flow.

(5) From the mathematical analysis of the spatially varied flow passing over the bottom rack by use of the theory of the singular point it is concluded that the singular point becomes a nodal point for $h_c/B < 1/6$ and a saddle one for $h_c/B > 1/6$, and that the three-dimensional problem of the spatially varied flow is reduced to a two-dimensional one in the $Q-h$ or $h-x$ phase plane.

(6) When a quasi-saddle point appears near the entrance the flow behaviour on the diversion structure is determined by only the initial discharge rate, bed slope, opening ratio and the distance from the entrance. The analysis of flow profile by use of the gradually and rapidly varied flow theory provides some information about the evaluation of the elements to be considered in flow analysis.

Acknowledgements

Bibliography

1) Hinds, J.: Side Channel Spillways; Hydraulic Theory, Economic Factors and Experimental Determination of Losses, Trans., A. S. C. E., Vol. 89, 1926, pp. 881–927.

2) Favre, H.: Contribution à l'étude des courants liquides, Dunod, Paris, 1933.

3) Camp, T. R.: Lateral Spillway Channels, Trans. A. S. C. E., Vol. 105, 1940, pp. 606–617.

4) Miller, C. N.: An Approximate Formula for Calculating the Design Capacity of Rapid Sand Filter Wash Water Troughs, Appendix B in Ellms, J. W. "Water Purification", Mc Graw-Hill Book Co., Inc., New York, 1928.

5) Stein, M. F.: The Design of Wash Water Troughs for Rapid Sand Filters, Jour., A. W. W. A., Vol. 13, 1925, pp. 411–415.

6) Werner, P. W.: Wasserspiegelberechung von Kanälen bei gleichmässiger Bewegung und veränderlicher Wassermenge, Die Bautechnik, Berlin, Vol. 19, No. 23, 1941, pp. 251–253.

7) Homma, M.: A Computation of Flow Profile with Lateral Inflow, Kensetsu-Kogaku, Vol. 2, No. 1, 1949 (in Japanese).

8) De Marchi, G.: Saggio di teoria del funzionamento degli stramazzi laterali, L'Energia Elettrica, Milano, Vol. 11, No. 11, 1934, pp. 849–860.

9) Gentilini, B.: Ricerche sperimentali sugli sfioratori longitudinali, L'Energia Elettrica, Milano, Vol. 15, No. 9, 1938, pp. 583–595.

10) Noseda, G.: Operation and Design of Bottom Intake Racks, Proc., 6th General Meeting, I. A. H. R., The Hague, 1955.

11) Kuntzmann, J. and Bouvard, M.: Étude théorique des grilles de prises d'eau du type "endessous", La Houille Blanche, Grenoble, 9th yr., No. 5, 1954, pp. 569–574.

12) Frank, J.: Hydraulische Untersuchungen für das Tiroler Wehr, Der Bauingenieur, Berlin, Vol. 31, No. 3, 1956, pp. 96–101.

13) Iwasa, Y.: The Fundamental Theory of Open Channel Flow, Water Works Series, 64-01, The Hydraulic Committee, The Japan Society of Civil Engineers, 1964 (in Japanese).

14) Iwasa, Y.: Theoretical Study of Hydraulic Behaviour of Boundary Characteristics to Channel Transitions and Controls in Divergent or Convergent Channel, Trans. J. S. C. E., Vol. 59, Sep. No. 3-1, 1958.